Open access • Journal Article • DOI:10.1103/PHYSREVLETT.112.242501

Observation of a p-Wave One-Neutron Halo Configuration in 37Mg — Source link

Nagao Kobayashi, Takashi Nakamura, Yosuke Kondo, J. A. Tostevin ...+28 more authors

Institutions: Tokyo Institute of Technology, Japan Atomic Energy Agency, Western Michigan University, Saint Mary's University ...+4 more institutions

Published on: 18 Jun 2014 - Physical Review Letters (American Physical Society)

Topics: Halo nucleus, Neutron, Island of inversion, Nucleon and Halo

Observation of a p-Wave One-Neutron Halo Configuration in ^{37}Mg

N. Kobayashi,[1,*] T. Nakamura,[1] Y. Kondo,[1] J. A. Tostevin,[2,1] Y. Utsuno,[3] N. Aoi,[4,†] H. Baba,[4] R. Barthelemy,[5] M. A. Famiano,[5] N. Fukuda,[4] N. Inabe,[4] M. Ishihara,[4] R. Kanungo,[6] S. Kim,[7] T. Kubo,[4] G. S. Lee,[1] H. S. Lee,[7] M. Matsushita,[4,‡] T. Motobayashi,[4] T. Ohnishi,[4] N. A. Orr,[8] H. Otsu,[4] T. Otsuka,[9] T. Sako,[1] H. Sakurai,[4] Y. Satou,[7] T. Sumikama,[10,§] H. Takeda,[4] S. Takeuchi,[4] R. Tanaka,[1] Y. Togano,[4,¶] and K. Yoneda[4]

[1]*Department of Physics, Tokyo Institute of Technology, 2-12-1 O-Okayama, Meguro, Tokyo 152-8551, Japan*
[2]*Department of Physics, Faculty of Engineering and Physical Sciences, University of Surrey, Guildford, Surrey GU2 7XH, United Kingdom*
[3]*Japan Atomic Energy Agency, Tokai, Ibaraki 319-1195, Japan*
[4]*RIKEN Nishina Center, Hirosawa 2-1, Wako, Saitama 351-0198, Japan*
[5]*Department of Physics, Western Michigan University, Kalamazoo, Michigan 49008, USA*
[6]*Astronomy and Physics Department, Saint Mary's University, Halifax, Nova Scotia B3 H 3C3, Canada*
[7]*Department of Physics and Astronomy, Seoul National University, Seoul 151-742, Korea*
[8]*LPC-Caen, ENSICAEN, IN2P3-CNRS, Université de Caen, 14050 Caen Cedex, France*
[9]*CNS, University of Tokyo, RIKEN Campus, Wako, Saitama 351-0198, Japan*
[10]*Department of Physics, Tokyo University of Science, Chiba 278-8510, Japan*

(Received 13 March 2014; published 18 June 2014)

Cross sections of $1n$-removal reactions from the neutron-rich nucleus ^{37}Mg on C and Pb targets and the parallel momentum distributions of the ^{37}Mg residues from the C target have been measured at 240 MeV/nucleon. A combined analysis of these distinct nuclear- and Coulomb-dominated reaction data shows that the ^{37}Mg ground state has a small $1n$ separation energy of $0.22^{+0.12}_{-0.09}$ MeV and an appreciable p-wave neutron single-particle strength. These results confirm that ^{37}Mg lies near the edge of the "island of inversion" and has a sizable p-wave neutron halo component, the heaviest such system identified to date.

DOI: 10.1103/PhysRevLett.112.242501 PACS numbers: 24.50.+g, 21.10.Jx, 25.60.Gc

Nuclear halo formation is an important feature of nuclei with extreme neutron to proton number asymmetry near the limits of nuclear stability [1–5]. The halo, a dilute neutron cloud of large radius, has a small spatial overlap with a core of more tightly bound nucleons [6–8]. Necessary conditions for halo formation are that one or two valence neutrons have (a) weak binding, with typical separation energies $S_n < 1$ MeV, which are significantly lower than the more conventional 8 MeV, and (b) low orbital angular momenta, $\ell = 0$ or 1 [2]. The reactions of nuclei with such spatially extended halo distributions lead to several interesting phenomena such as soft $E1$ excitations [9], narrow momentum distributions of the core fragments following dissociation, reflecting low Fermi momenta of the halo neutron(s) [5,7,8], and large reaction cross sections [5,6].

Very recently, the formation of halo configurations was also found to be strongly correlated with other aspects of the structure of neutron-rich nuclei, such as shell evolution and the presence of deformation [10,11]. Formation of such halo components, with their low kinetic energy content, may impart added stability, affecting the location of the drip line, the limit of binding in neutron-rich nuclei [11].

Despite this significance of halo features for nuclear structure studies, the experimental difficulties in accessing the extremes of neutron-rich nuclei have restricted the confirmed neutron-halo cases to the light neutron-rich sector of the nuclear chart, namely, in p- and sd-shell nuclei with $N < 20$. The notable exception is the recently confirmed $1n$-halo nature of ^{31}Ne [10–12]. The ^{31}Ne ground state was shown to have a p-wave halo component, built upon the $^{30}\mathrm{Ne}(0^+_1)$ core [11], with about 30% of a single-particle strength, very different from the lighter, more conventional $1n$-halo nuclei with their dominant s-wave configurations [5,9]. This deduced ^{31}Ne structure was strongly suggestive of the presence of deformation [11], the halo formation being driven by the nuclear Jahn-Teller effect due to the near degeneracy of the $\nu 1f_{7/2}$ and $\nu 2p_{3/2}$ orbitals [13–15]. However, the role of such interplay between shell evolution, deformation, and halo formation remains an open question for heavier near-drip-line nuclei. Here we consider ^{37}Mg.

Almost no experimental information is available for ^{37}Mg ($Z = 12$, $N = 25$), the most neutron-rich bound odd-mass Mg isotope and member of the $N = 25$ isotonic chain, beyond its first identification [16]. Neither its half-life, ground state ($^{37}\mathrm{Mg}_{\mathrm{g.s}}$) spin parity, nor its mass have been measured; although mass systematics suggest that it is very weakly bound $S_n = 0.16(68)$ MeV, albeit with a relatively large uncertainty [17]. Thus ^{37}Mg is a candidate for a $1n$-halo system that is heavier than ^{31}Ne [10–12]. This Letter reports evidence of such a neutron halo component in ^{37}Mg. In the conventional, spherical shell model, the

$^{37}\mathrm{Mg}_{\mathrm{g.s.}}$ would have $J^\pi = 7/2^-$, the least bound neutron occupying the $1f_{7/2}$ orbital, and the resulting high centrifugal barrier would then suppress halo formation. So, evidence for the existence of halolike structure would imply significant modifications to this shell structure and the likely presence of deformation.

^{37}Mg is also important in understanding how the feature of the *island of inversion* (IoI) evolves from $N = 20$ to $N = 28$. A nucleus in the IoI is characterized by significant components of $2\hbar\omega$, $2p-2h$ $[\nu(sd)^{-2}(fp)^{+2}]$ neutron *intruder* configurations and thus is deformed [18]. The well-established picture of the IoI around ^{34}Mg ($N = 22$) [19,20], where $2\hbar\omega$ configurations are dominant in the ground state, may change towards $N = 28$. ^{36}Mg was recently confirmed to be within the IoI, but with reduced $2\hbar\omega$ contributions [21], suggesting a transitional behavior of the neighboring ^{37}Mg nucleus. A recent in-beam γ-ray experiment on ^{38}Mg, however, confirmed that ^{38}Mg is as well deformed as ^{34,36}Mg [22], suggesting a more constant structural behavior towards $N = 28$. Hence, the evolution of IoI features toward $N = 28$ is of importance, and investigation of the odd-A nucleus ^{37}Mg gives greater sensitivity and insight into the active single-particle states.

The present work addresses this spectroscopy of neutron-rich nuclei near the edge of the IoI. Specifically, the halo, shell, and deformation properties of $^{37}\mathrm{Mg}_{\mathrm{g.s.}}$ are deduced by using Coulomb- and nuclear-dominated $1n$-removal reactions at energies around 240 MeV/nucleon, exploiting their distinctive sensitivities to the asymptotic wave function of the active single-particle states [9,23,24]. Hence, as demonstrated in the recent work on ^{31}Ne [11], a combined analysis of data for these reactions allows one to extract S_n, J^π, and the spectroscopic factor C^2S of the $\langle {}^{36}\mathrm{Mg}(0_1^+)|{}^{37}\mathrm{Mg}_{\mathrm{g.s.}}\rangle$ overlap.

The experiment was performed at the RI Beam Factory (RIBF) [25] at RIKEN. The Superconducting Ring Cyclotron supplied a ^{48}Ca primary beam at 345 MeV/nucleon with the beam intensity $\approx$100 pnA. The ^{37}Mg secondary beam, produced by projectile fragmentation at a 15-mm-thick rotating Be target, had typical intensity of 6 pps and a momentum spread ($\Delta P/P$) of $\pm 3\%$. Each ^{37}Mg particle was identified according to the magnetic rigidity ($B\rho$), time of flight (TOF), and energy loss (ΔE) obtained by the standard detectors of the fragment separator BigRIPS [26,27]. The midtarget energies of the $1n$-removal reactions were 244 MeV/nucleon for the Pb target (3.37 g/cm^2) and 240 MeV/nucleon for the C target (2.54 g/cm^2). The ^{36}Mg residues produced were identified by their $B\rho$, TOF, and ΔE measured with the Zero Degree Spectrometer [26,27]. In addition, the γ-ray detector array DALI2 [22,28] was installed, surrounding the reaction target, to detect γ rays emitted from those ^{36}Mg residues populated in excited states.

The first row of Table I shows the inclusive $1n$-removal cross sections on C [σ_{-1n}(C)], on Pb [σ_{-1n}(Pb)], and the estimated Coulomb breakup contribution [$\sigma_{-1n}(E1)$] on the Pb target. The latter is obtained by subtracting a nuclear contribution, estimated by scaling the σ_{-1n}(C) value [10,11]. The large deduced $\sigma_{-1n}(E1)$ value of about 0.5 b, comparable to that for established $1n$-halo systems such as ^{19}C and ^{31}Ne [10], is indicative of a soft $E1$ excitation and $1n$-halo component in ^{37}Mg.

TABLE I. Measured $1n$-removal cross sections of ^{37}Mg on C [σ_{-1n}(C)] and Pb [σ_{-1n}(Pb)] and the extracted Coulomb breakup contribution on Pb [$\sigma_{-1n}(E1)$]. The three rows show the inclusive $1n$-removal cross sections, the partial cross sections for excited states decaying via the 662-keV γ ray, and the partial cross sections for direct feeding of the $^{36}\mathrm{Mg}(0_1^+)$.

Reaction	σ_{-1n}(C) [mb]	σ_{-1n}(Pb) [mb]	$\sigma_{-1n}(E1)$ [mb]
(^{37}Mg, ^{36}Mg) (inclusive)	80(4)	660(40)	490(50)
(^{37}Mg, ^{36}Mg*)	42(7)	130(50)	40(60)
[^{37}Mg, $^{36}\mathrm{Mg}(0_1^+)$]	38(8)	530(60)	450(80)

To examine this neutron halo component quantitatively, the inclusive cross section σ_{-1n} is resolved into partial cross sections feeding the $^{36}\mathrm{Mg}(0_1^+)$ and bound excited states (^{36}Mg*) using the γ rays measured in coincidence with the ^{36}Mg residues. Figure 1 shows these Doppler-shift-corrected γ-ray coincidence spectra for the C and Pb targets. A peak near 660 keV is observed, corresponding to the known $2_1^+ \rightarrow 0_1^+$ transition [21,22]. For the C target [Fig. 1(a)], we also see the hint of a second peak near 1400 keV that can be assigned to the recently observed $4_1^+ \rightarrow 2_1^+$ transition [22]. By fixing these energies to the known values 662 and 1370 keV [22], the γ-ray spectrum on the C target is fitted with the detector response function for these transitions, obtained from a GEANT4 simulation, plus an assumed exponentially decreasing background. This is shown in Fig. 1(a). For the Pb target [Fig. 1(b)], only the 662-keV transition is evident. Table I also presents the deduced partial cross sections for direct feeding of the $^{36}\mathrm{Mg}(0_1^+)$ for the C and Pb targets, now denoted

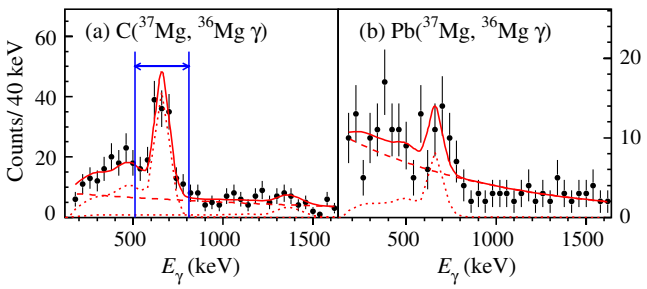

FIG. 1 (color online). Measured γ-ray spectra in coincidence with ^{36}Mg residues following $1n$ removal from ^{37}Mg on C (a) and Pb (b) targets. The solid red lines show the fits to the spectra based on the simulated detector response functions (dotted red lines) and exponential backgrounds (dashed red lines).

$\sigma_{-1n}(\mathrm{C};0_1^+)$ and $\sigma_{-1n}(\mathrm{Pb};0_1^+)$, respectively, obtained by subtracting the values for the $2_1^+ \to 0_1^+$ transition, of the second row, from the inclusive cross sections. The partial cross section feeding $^{36}\mathrm{Mg}(0_1^+)$ due to Coulomb breakup, $\sigma_{-1n}(E1;0_1^+)$, is obtained similarly.

To assess the characteristics of the valence neutron removed from $^{37}\mathrm{Mg}_{\mathrm{g.s}}$, we subject these deduced nuclear and Coulomb breakup partial cross sections $\sigma_{-1n}(\mathrm{C};0_1^+)$ and $\sigma_{-1n}(E1;0_1^+)$ to a combined analysis [11]. We interrogate both the ground state to ground state S_n and C^2S by taking the ratios of the experimental and calculated cross sections. For the C target and each assumed S_n, an empirical spectroscopic factor $C^2S(0_1^+;n\ell j)$ for removal from a given neutron single-particle state is deduced from the ratio of $\sigma_{-1n}(\mathrm{C};0_1^+)$ to the calculated single-particle cross section $\sigma_{\mathrm{sp}}(\mathrm{C};n\ell j)$. These $\sigma_{\mathrm{sp}}(\mathrm{C};n\ell j)$ are computed by using the eikonal model [23]. Similarly, for the Pb target data, the ratio of $\sigma_{-1n}(E1;0_1^+)$ to $\sigma_{\mathrm{sp}}(E1;n\ell j)$ is used to make a second, independent $C^2S(0_1^+;n\ell j)$ assignment, where the required $\sigma_{\mathrm{sp}}(E1;n\ell j)$ values are obtained by using the direct Coulomb-breakup model of Ref. [11].

Figure 2 presents these two independently determined C^2S as a function of S_n, assuming neutron removal from (a) $2s_{1/2}$, (b) $2p_{3/2}$, (c) $1d_{3/2}$, and (d) $1f_{7/2}$ orbitals. These correspond to $^{37}\mathrm{Mg}_{\mathrm{g.s}}(J^\pi)$ of $1/2^+$, $3/2^-$, $3/2^+$, and $7/2^-$, respectively. The results for $2p_{1/2}$, $1d_{5/2}$, and $1f_{5/2}$ orbitals are almost identical to those shown in Figs. 2(b), 2(c), and 2(d), respectively. The blue and red areas show the C^2S from the $\sigma_{-1n}(\mathrm{C};0_1^+)$ and the $\sigma_{-1n}(E1;0_1^+)$ analyses, with their experimental error bands, and so regions of overlap represent those C^2S and S_n consistent with the reaction models used and the data. Figure 2(d) shows there is no such overlap for f-wave neutron removal which is thus excluded. Figure 2(c) shows that any overlap for a d-wave neutron is at the limits of the error bars on the data sets and requires a pure d-wave configuration, $^{36}\mathrm{Mg}(0_1^+) \otimes 1d_{3/2}$, with $C^2S \approx 1$ and $S_n \approx 0$ MeV. However, such a configuration is not realized in the mass region around ^{37}Mg. The s- and p-wave cases, on the other hand, have well-defined regions of overlap. A chi-squared analysis of the $2p_{3/2}$ case, of Fig. 2(b), gives the values $S_n = 0.22^{+0.12}_{-0.09}$ MeV and $C^2S = 0.42^{+0.14}_{-0.12}$. The values for $2p_{1/2}$ are essentially identical. For the s-wave case [Fig. 2(a)], the corresponding results are $S_n = 0.40^{+0.19}_{-0.13}$ MeV and $C^2S = 0.40^{+0.16}_{-0.13}$. Thus, from Fig. 2, the most probable $^{37}\mathrm{Mg}_{\mathrm{g.s}}$ spin parity assignments are $3/2^-$, $1/2^-$, and $1/2^+$, corresponding to the $^{36}\mathrm{Mg}(0_1^+) \otimes 2p_{3/2}$, $^{36}\mathrm{Mg}(0_1^+) \otimes 2p_{1/2}$, and $^{36}\mathrm{Mg}(0_1^+) \otimes 2s_{1/2}$ configurations, respectively, in the ground state to ground state overlap. The deduced S_n values are consistent with the evaluated value 0.16 (68) MeV [17], but with an improved accuracy.

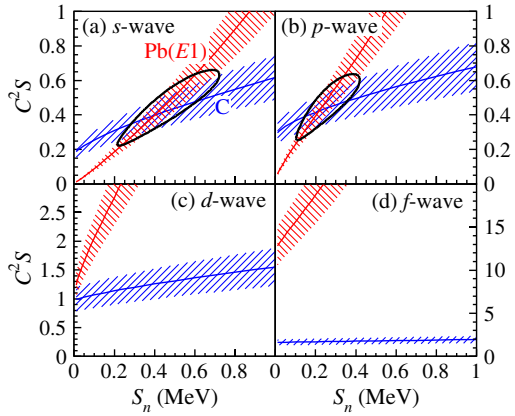

FIG. 2 (color online). The blue and red hatched areas show the C^2S values deduced from the data, as a function of S_n. (a)–(d) show the results assuming $2s_{1/2}$, $2p_{3/2}$, $1d_{3/2}$, and $1f_{7/2}$ neutron removal, respectively, from $^{37}\mathrm{Mg}_{\mathrm{g.s}}$. The thick black lines in (a) and (b) represent the deduced region of overlap with a 68% confidence level.

These assessments are also confronted with large-scale shell model (SM) calculations that employ the $sd-pf$ cross shell, modified monopole (SDPF-M) SM effective interaction [29]. Additionally, the $2p_{1/2}$ orbital is included in the SM model space to generate a realistic $^{36}\mathrm{Mg}(0_1^+) \otimes 2p_{1/2}$ configuration and overlap. Table II compares the experimental and theoretical cross sections on the C target when making the $3/2^-$, $1/2^-$, or $1/2^+$ $^{37}\mathrm{Mg}_{\mathrm{g.s}}$ SM assignments. The theoretical values are computed by using the eikonal reaction model and the SM C^2S values from the $\langle ^{36}\mathrm{Mg}(J^\pi)|^{37}\mathrm{Mg}_{\mathrm{g.s}}\rangle$ overlaps. The calculations include the

TABLE II. Experimental inclusive and partial $1n$-removal cross sections on C [$\sigma_{-1n}(\mathrm{C})$] are compared with eikonal model calculations [$\sigma^{\mathrm{th}}_{-1n}(\mathrm{C})$] using the SM C^2S values for an assumed $3/2^-$, $1/2^-$, or $1/2^+$ ^{37}Mg ground state. The theoretical cross sections shown for $^{36}\mathrm{Mg}^* \otimes 2p$, $^{36}\mathrm{Mg}^* \otimes 1f$, and $^{36}\mathrm{Mg}^* \otimes 1d$ are the sums of cross sections to all bound excited final states $^{36}\mathrm{Mg}^*$ that originate from p-, f-, and d-state neutron SM configurations in $^{37}\mathrm{Mg}_{\mathrm{g.s}}$.

Configuration	σ_{sp} (mb)	C^2S	$\sigma^{\mathrm{th}}_{-1n}(\mathrm{C})$ (mb)	$\sigma_{-1n}(\mathrm{C})$ (mb)
C[$^{37}\mathrm{Mg}(3/2^-)$, ^{36}Mg]				
$^{36}\mathrm{Mg}(0_1^+) \otimes 2p_{3/2}$	89.4	0.31	30.1	38(8)
$^{36}\mathrm{Mg}^* \otimes 2p$	⋯	0.47	17.4	
$^{36}\mathrm{Mg}^* \otimes 1f$	⋯	1.35	23.0	
Inclusive			80.6	80(4)
C[$^{37}\mathrm{Mg}(1/2^-)$, ^{36}Mg]				
$^{36}\mathrm{Mg}(0_1^+) \otimes 2p_{1/2}$	88.1	0.20	18.9	38(8)
$^{36}\mathrm{Mg}^* \otimes 2p$	⋯	0.44	17.4	
$^{36}\mathrm{Mg}^* \otimes 1f$	⋯	1.80	28.4	
Inclusive			77.6	80(4)
C[$^{37}\mathrm{Mg}(1/2^+)$, ^{36}Mg]				
$^{36}\mathrm{Mg}(0_1^+) \otimes 2s_{1/2}$	95.3	0.001	0.1	38(8)
$^{36}\mathrm{Mg}^* \otimes 1d$	⋯	0.85	15.7	
$^{36}\mathrm{Mg}^* \otimes 2p$	⋯	0.17	5.1	
$^{36}\mathrm{Mg}^* \otimes 1f$	⋯	1.00	15.4	
Inclusive			37.0	80(4)

predicted bound SM excited states of ^{36}Mg up to the energy $S_n(^{36}\mathrm{Mg}) = 3.33(49)$ MeV [17]. For the $3/2^-$ case, the actual SM ground state, the measured inclusive and partial cross sections are reproduced by the calculations, supporting this assignment. The partial cross sections for the alternative $1/2^-$ assignment are less well reproduced, but the assignment is not excluded by the SM energy, of 0.28 MeV, or the final-state inclusive cross section. The $1/2^+$ ground state assignment of Fig. 2(a) is very unlikely. The large measured ground state partial cross section contradicts the SM calculation that, due to the almost complete occupancy of the $\nu 2s_{1/2}$ orbital in the ^{36}Mg core, suppresses such an overlap and transition. This lowest $1/2^+$ state lies at 1.37 MeV above the SM ground state, too high to be accommodated by reasonable modifications to the SM.

We conclude therefore that the $^{37}\mathrm{Mg}_{\mathrm{g.s}}$ has a significant weakly bound $J^\pi = 3/2^-$ or $1/2^-$ p-wave halo component with a $^{36}\mathrm{Mg}(0_1^+) \otimes 2p_J$ configuration.

Figure 3 shows, for the C target, the parallel momentum distributions of the ^{36}Mg reaction residues, in the rest frame of the ^{37}Mg projectile, observables that permit further examination of the orbital angular momentum of the removed neutron [23]. Figure 3(a) shows the inclusive momentum distribution and Fig. 3(b) the distribution for events in coincidence with γ rays with $510 < E_\gamma < 810$ keV, shown by an arrow in Fig. 1. The latter corresponds to all events that populate $^{36}\mathrm{Mg}^*$ final states. The width of the inclusive momentum distribution of $82(13)$ MeV/c, extracted from a fit with a Lorentzian folded by the experimental resolution, indicates the importance of low-ℓ orbital components in $^{37}\mathrm{Mg}_{\mathrm{g.s}}$. The measured distributions are compared with the eikonal model predictions for the p-wave configurations with $J^\pi = 3/2^-$ and $1/2^-$. These are constructed by weighting the individual calculations to each bound SM final state by its C^2S value. So, Fig. 3(a) includes and Fig. 3(b) excludes the $^{36}\mathrm{Mg}(0_1^+)$ contribution to these sums. The thick (thin) lines represent the results for the $3/2^-$ ($1/2^-$) SM state. The total contributions of p- and f-state neutron removal to these cross sections are shown by the red dashed and blue dotted lines, respectively. The sums of all contributions, the black lines, should be compared to the data where, as above, the thin lines assume the $1/2^-$ SM state.

The shapes of the experimental distributions are reproduced by the calculations for the p-wave configurations. The distributions reveal the importance of the p-wave neutron contributions to the $\langle ^{36}\mathrm{Mg}(0_1^+)|^{37}\mathrm{Mg}_{\mathrm{g.s}}\rangle$ overlap for reproducing the measured data for the $^{37}\mathrm{Mg}_{\mathrm{g.s}}$ to $^{36}\mathrm{Mg}(0_1^+)$ transition, at odds with the expectation of the naive spherical shell model. This indicates a breakdown of the conventional shell ordering and deformation in ^{37}Mg. The quality of agreement with the realistic SM calculation supports such a deformation picture, since the SM $^{37}\mathrm{Mg}_{\mathrm{g.s}}$ involves complex mixing of configurations, as shown in Table II.

The deformation of ^{37}Mg can be understood in terms of $2\hbar\omega$ intruder configurations in $^{37}\mathrm{Mg}_{\mathrm{g.s}}$ (IoI picture). Figure 4 shows the evolution of the fractions (as percent) of $0\hbar\omega$ and $2\hbar\omega$ configurations in the ground states of the Mg isotopes, obtained from the SM calculations discussed above. The figure indicates that ^{37}Mg and ^{36}Mg are located in the region where the $0\hbar\omega$ and $2\hbar\omega$ configurations are strongly mixed and different from the behavior near $N = 20$. Indeed, it was recently quantified that $^{36}\mathrm{Mg}(0_1^+)$ has 38(8)% of $0\hbar\omega$ configurations [21]. For ^{37}Mg, the agreement of the current cross sections and momentum distributions with the SM results provides evidence for such intruder configurations. Turning off the $2\hbar\omega$ components in $^{37}\mathrm{Mg}_{\mathrm{g.s}}$ would produce smaller $1n$-removal yields due to the blocking of the decays of these $2\hbar\omega$ $^{36}\mathrm{Mg}(0_1^+)$ components. The existence of such intruder configurations places $^{37}\mathrm{Mg}_{\mathrm{g.s}}$ within but near the edge of the IoI. We note also that the current SM calculations predict that the IoI may have a long shore towards ^{40}Mg ($N = 28$). To clarify the entire picture along the isotopic chain, further investigations of the heavier Mg isotopes will be necessary.

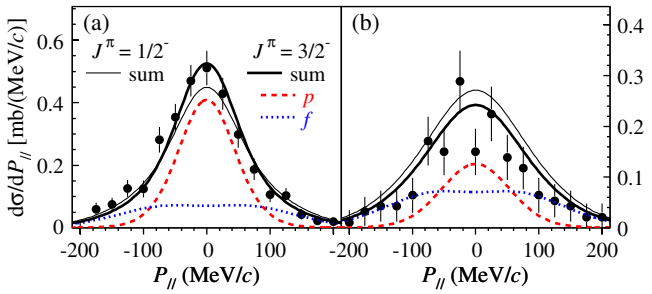

FIG. 3 (color online). Measured parallel momentum distributions of ^{36}Mg residues and corresponding theoretical calculations using the $^{37}\mathrm{Mg}(3/2^-)$ (thick lines) and $^{37}\mathrm{Mg}(1/2^-)$ (thin lines) SM state calculation. (a) includes and (b) excludes the $^{36}\mathrm{Mg}(0_1^+)$ contribution to the inclusive distribution. The red dashed and blue dotted lines are the individual contributions from p- and f-wave neutron removal, respectively, and the black solid lines are the summed distributions.

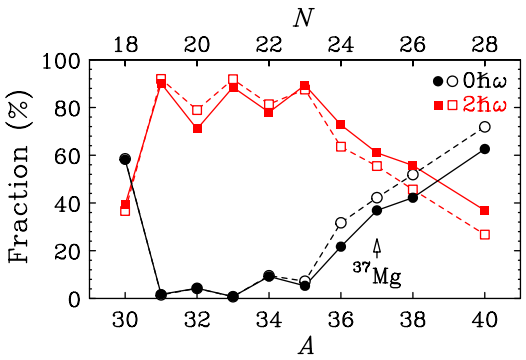

FIG. 4 (color online). The fractions of $0\hbar\omega$ (black circles) and $2\hbar\omega$ (red squares) configurations in the ground states of the Mg isotopes, as given by the SDPF-M (open symbols) [29] and SDPF − M + $p_{1/2}$ (solid symbols) large-scale SM calculations. The latter, used for the current analysis of ^{37}Mg, is more appropriate for nuclei near $N = 28$.

Another perspective on the mechanism driving deformation in ^{37}Mg is provided by the Jahn-Teller effect due to the near degeneracy of the $\nu 1f_{7/2}$ and $\nu 2p_{3/2}$ orbitals [11,13–15,30] and the melting of $N = 28$ magicity. The Nilsson diagram for ^{37}Mg (Fig. 5 of Ref. [13]), which shows this effect, indicates that the least-bound neutron will occupy the $[321]1/2^-$ state for quadrupole deformations $0.3 \leq \beta \leq 0.6$ and that the wave function is a strong mixture of pf-shell orbitals. Depending on the decoupling parameter, J^π is predicted to be $3/2^-$ for $0.30 \leq \beta \leq 0.34$ and $1/2^-$ for $0.34 \leq \beta \leq 0.60$, which is consistent with the present results. The near degeneracy of the $\nu 1f_{7/2}$ and $\nu 2p_{3/2}$ orbitals is thus expected to be correlated with characteristic behavior of weakly bound low-ℓ neutron single-particle configurations. This is in contrast to the (nearly) stable $N = 25$ isotones, such as $^{47}_{22}$Ti and $^{49}_{24}$Cr, which are deformed ($\beta = 0.2$–0.3) but their ground state bands correspond to the Nilsson $[312]5/2^-$ and $f_{7/2}$ dominant configuration [31] due to a large gap of $N = 28$.

In summary, we have presented a combined analysis of the data from Coulomb- and nuclear-dominated $1n$-removal reactions at 240 MeV/nucleon from ^{37}Mg. An extremely small ground state to ground state separation energy $S_n = 0.22^{+0.12}_{-0.09}$ MeV and a spectroscopic factor for $p_{3/2}$ neutron removal of $C^2S = 0.42^{+0.14}_{-0.12}$ are deduced. The $J^\pi = 3/2^-$ ^{37}Mg spin assignment is most likely, but the $J^\pi = 1/2^-$ assignment is not fully excluded. All of the results presented are consistent with a picture in which ^{37}Mg is deformed and has a significant ($\approx 40\%$) p-wave neutron halo component. Furthermore, the results are consistent with large-scale SM calculations that suggest ^{37}Mg$_{g.s}$ lies within the island of inversion, that is responsible for the deformation, but with a reduced fraction of $2\hbar\omega$ intruder configurations. The nuclear Jahn-Teller effect, driven by the fp-orbital degeneracy (melting of $N = 28$ magicity) in weakly bound nuclei, may also play a role in the deformation. To complete the picture, halo phenomena and shell evolution should be investigated towards $N = 28$ and beyond on the neutron drip line.

We thank the RIKEN accelerator staff for the excellent beam delivery and fruitful discussions with I. Hamamoto. The RIBF is operated by the RIKEN Nishina Center and the Center for Nuclear Study (CNS), University of Tokyo. The present work was supported in part by JSPS KAKENHI Grant No. 22340053, MEXT KAKENHI Grant No. 24105005, and NRF grant [R32-2008-000-10155-0 (WCU)] of MEST Korea. N. K. acknowledges the Grant-in-Aid support by JSPS (No. 25·10601). J. A. T. acknowledges support of the Science and Technology Facilities Council (United Kingdom) Grant No. ST/J000051. N. A. O. acknowledges support from the Franco-Japanese LIA-International Associated Laboratory for Nuclear Structure Problems. R. K. acknowledges support from NSERC.

*Present address: Department of Physics, University of Tokyo, 7-3-1 Hongo, Bunkyo, Tokyo 113-0033, Japan.
†Present address: RCNP, Osaka University, Mihogaoka, Ibaraki, Osaka 567-0047, Japan.
‡Present address: CNS, University of Tokyo, RIKEN Campus, Wako, Saitama 351-0198, Japan.
§Present address: Department of Physics, Tohoku University, Miyagi 980-8578, Japan.
¶Present address: Department of Physics, Tokyo Institute of Technology, 2-12-1 O-Okayama, Meguro, Tokyo 152-8551, Japan.

[1] I. Tanihata, Prog. Part. Nucl. Phys. **35**, 505 (1995).
[2] A. S. Jensen, K. Riisager, D. V. Fedorov, and E. Garrido, Rev. Mod. Phys. **76**, 215 (2004).
[3] B. Jonson, Phys. Rep. **389**, 1 (2004).
[4] T. Frederico, A. Delfino, L. Tomio, and M. T. Yamashita, Prog. Part. Nucl. Phys. **67**, 939 (2012).
[5] I. Tanihata, H. Savajols, and R. Kanungo, Prog. Part. Nucl. Phys. **68**, 215 (2013).
[6] I. Tanihata, H. Hamagaki, O. Hashimoto, Y. Shida, N. Yoshikawa, K. Sugimoto, O. Yamakawa, T. Kobayashi, and N. Takahashi, Phys. Rev. Lett. **55**, 2676 (1985).
[7] T. Kobayashi, O. Yamakawa, K. Omata, K. Sugimoto, T. Shimoda, N. Takahashi, and I. Tanihata, Phys. Rev. Lett. **60**, 2599 (1988).
[8] N. A. Orr *et al.*, Phys. Rev. Lett. **69**, 2050 (1992).
[9] T. Aumann and T. Nakamura, Phys. Scr. **T152**, 014012 (2013).
[10] T. Nakamura *et al.*, Phys. Rev. Lett. **103**, 262501 (2009).
[11] T. Nakamura *et al.*, Phys. Rev. Lett. **112**, 142501 (2014).
[12] M. Takechi *et al.*, Phys. Lett. B **707**, 357 (2012).
[13] I. Hamamoto, Phys. Rev. C **76**, 054319 (2007).
[14] I. Hamamoto, Phys. Rev. C **81**, 021304(R) (2010).
[15] I. Hamamoto, Phys. Rev. C **85**, 064329 (2012).
[16] H. Sakurai *et al.*, Phys. Rev. C **54**, R2802 (1996).
[17] M. Wang, G. Audi, A. H. Wapstra, F. G. Kondev, M. MacCormick, X. Xu, and B. Pfeiffer, Chin. Phys. C **36**, 1603 (2012).
[18] E. K. Warburton, J. A. Becker, and B. A. Brown, Phys. Rev. C **41**, 1147 (1990).
[19] H. Iwasaki *et al.*, Phys. Lett. B **522**, 227 (2001).
[20] K. Yoneda *et al.*, Phys. Lett. B **499**, 233 (2001).
[21] A. Gade *et al.*, Phys. Rev. Lett. **99**, 072502 (2007).
[22] P. Doornenbal *et al.*, Phys. Rev. Lett. **111**, 212502 (2013).
[23] P. G. Hansen and J. A. Tostevin, Annu. Rev. Nucl. Part. Sci. **53**, 219 (2003), and references therein.
[24] N. Kobayashi *et al.*, Phys. Rev. C **86**, 054604 (2012).
[25] Y. Yano, Nucl. Instrum. Methods Phys. Res., Sect. B **261**, 1009 (2007).
[26] T. Kubo, Nucl. Instrum. Methods Phys. Res., Sect. B **204**, 97 (2003).
[27] T. Kubo *et al.*, IEEE Trans. Appl. Supercond. **17**, 1069 (2007).
[28] S. Takeuchi *et al.*, Phys. Rev. Lett. **109**, 182501 (2012).
[29] Y. Utsuno, T. Otsuka, T. Mizusaki, and M. Honma, Phys. Rev. C **60**, 054315 (1999).
[30] Y. Utsuno, T. Otsuka, B. Alex Brown, M. Honma, T. Mizusaki, and N. Shimizu, Phys. Rev. C **86**, 051301(R) (2012).
[31] F. Brandolini and C. A. Ur, Phys. Rev. C **71**, 054316 (2005).